

Evidence for cold baryonic matter fueling the Milky Way deduced from the first detection of dust emission in High-Velocity Clouds

M.-A. Miville-Deschênes^{1,2}, F. Boulanger¹, W. T. Reach³ & A. Noriega-Crespo³

April 12, 2005

1. Institut d'Astrophysique Spatiale, Université Paris-XI, 91405, Orsay Cedex, France
2. Canadian Institute for Theoretical Astrophysics, University of Toronto, 60 St-George st, Toronto, Canada
3. Infrared Processing and Analysis Center, California Institute of Technology, Pasadena, CA 91125, USA

Abstract

Since their discovery in HI observations[1], High Velocity Clouds (HVCs) keep being the puzzling targets of numerous studies (see ref. 2 for a thorough review). It is now widely considered that a large fraction of them might be primordial infalling clouds fueling the Galaxy with low metallicity gas. This hypothesis received strong support from FUSE observations that showed that most HVCs have a subsolar metallicity[3] and a D/H ratio compatible with primordial abundances of deuterium[4]. By comparing sensitive 21 cm and infrared observations we made the first detection of dust emission in Complex C, the largest HVC on the sky. The observations could be explained by very unusual dust properties or, based on the metallicity measurements and assuming diffuse Galactic interstellar medium (ISM) dust/metals ratio, this detection could imply gas column densities more than one order of magnitude higher than that observed in HI and H+ gas. The infall of this previously undetected baryonic mass would be enough to account for the distribution of stellar metallicities with age, to maintain bars[5] and to fuel star formation in Milky Way type galaxies.

The present study focuses on the Spitzer Extra-Galactic First Look Survey (XFLS) field, a diffuse HI area ($N_{HI} \sim 2 \times 10^{20} \text{ cm}^{-2}$) at high Galactic latitude ($l = 88^\circ.3$, $b = 34^\circ.9$) that is used as an extra-galactic window to study galaxy populations and galaxy clustering with Spitzer[6]. The XFLS field is located on the edge of Complex C that spans more than 1500 square degrees on the sky. Complex C has a subsolar metallicity ($\sim 0.1 - 0.3$)[7], it contains ionised gas observed in emission[8] ($H\alpha$) and absorption[9] (O VI) and it is located at a distance greater than 5 kpc from the sun[10]. No dust emission has ever

been detected in HVCs[11, 12], in accordance with their H I column density, low metallicity (and therefore low dust/gas ratio) and their large distance (i.e. fainter radiation field). In this study we revisit the dust/gas correlation in HVCs using better 21 cm and infrared data.

We use 21 cm data obtained with the Green Bank Telescope (GBT), previously published and kindly made available by Lockman and Condon[13]. These observations cover a $3^\circ \times 3^\circ$ area centered at (J2000) $\alpha = 17^h 18^m$, $\delta = +59^\circ 30'$, which encloses the Spitzer observations. The GBT data were corrected for stray-radiation contamination. The beam of the GBT is $9'.2$ at 21 cm, the sampling was done at $1'.5$, the velocity resolution is 0.62 km s^{-1} and the noise level in a single channel is 0.05 K . Fig. 2 presents the 21 cm integrated emission map and the average spectrum of the XFLS field. On that figure one can also see the integrated emission of the Local gas ($-60 < v < 6.6 \text{ km s}^{-1}$) and of the High-Velocity ($-210 < v < -132 \text{ km s}^{-1}$) components.

The infrared maps come from two different datasets. First we use IRIS data[14] which are an improved version of the IRAS ISSA maps. We only use the 60 and $100 \mu\text{m}$ IRIS maps of the XFLS field as the 12 and $25 \mu\text{m}$ maps of this region have a residual instrumental contamination commensurate with the Galactic signal we are interested in. The FWHM angular resolution of the IRIS maps is $\sim 4'$ with a pixel size of $1'.5$. Second we use the Spitzer IRAC $8 \mu\text{m}$ and MIPS 24 and $160 \mu\text{m}$ data of the XFLS. The field was covered by IRAC in 9 raster map tiles. Each tile was low-pass-median-filtered to suppress individual galaxies; then the mosaics were combined, a polynomial surface subtracted to remove the zodiacal light, and the result was regridded to $16''$ pixels. The field was covered by MIPS in 8 scan maps that were combined and destriped, then regridded to $16''$ pixels and median-smoothed. Bright point sources were removed from all infrared maps before convolution by a Gaussian beam to bring them to the GBT $9'.2$ FWHM resolution. Fig. 1 shows the convolved maps.

The main goal of this study is to determine the infrared emissivity of Local and HVC HI components identified with the 21 cm observations. To do so we compared the two HI components to Spitzer and IRIS maps shown in Fig. 1. To estimate the emissivity of every HI components we considered that the infrared map $I_\lambda(x, y)$ at wavelength λ can be represented by the following model

$$I_\lambda(x, y) = e_\lambda^{Local} N_H^{Local}(x, y) + e_\lambda^{HVC} N_H^{HVC}(x, y) + C_\lambda(x, y) \quad (1)$$

where $N_H^i(x, y)$ is the column density of the i^{th} HI component, e_λ^i is the emissivity of component i at wavelength λ and $C_\lambda(x, y)$ is a term that regroups the Cosmic Infrared Background (CIB) and the instrumental noise. In our analysis we considered the two contributions to C_λ as Gaussian white noises.

To estimate e_λ^i we performed a multivariate regression based on the model given by Eq. 1. The emissivities found for each HI component and at each wavelength are collected in Table 1 and shown in Fig. 3. The striking result is certainly the first detection of the infrared emission associated with the HVC. In the following we will concentrate on this detection and leave the analysis of the local emissivities to another paper.

We model the far-IR dust emission of the HVC component within the Désert et al. model[15] including the contributions of stochastically heated Very Small Grains (VSG) and Big Grains (BG). BGs are in thermal equilibrium with the radiation field and therefore their emission follows a black body scaled by the emissivity. If we make the hypothesis that the extinction is lower than one, the emissivities (in $MJy/sr/10^{20}cm^{-2}$) given by the Desert et al. model[15] can be approximated by the following expression at wavelength where Polycyclic Aromatic Hydrocarbon (PAH) emission is not important:

$$e_{\lambda} = P_{vsg}C_{\lambda} + 2.0 \times 10^5 P_{bg}B(\lambda, T_{bg})\lambda^{-\beta} \quad (2)$$

The VSG emission scales with the radiation field strength (χ) and the VSG abundance (through the factor P_{vsg} , normalised to the local ISM value) and with always the same spectral shape ($C_{24\mu m} = 0.021$, $C_{60\mu m} = 0.099$, $C_{100\mu m} = 0.106$ and $C_{160\mu m} = 0.067$). The BG emission scales with P_{bg} which takes into account the variation with dust-to-gas mass ratio (Z_d) and FIR emissivity (Q_{FIR}) with respect to the local ISM value :

$$P_{bg} = q_{FIR} Z_d^{HVC} / Z_d^{ISM} \quad (3)$$

where $q_{FIR} = Q_{FIR}^{HVC} / Q_{FIR}^{ISM}$. The BG emission depends also on a modified black body function B where T_{bg} is the BG equilibrium temperature and $\beta \sim 2$ is the dust emissivity spectral index.

Assuming $\beta = 2$ we determined the unknown parameters of Eq. 2 (i.e. P_{vsg} , P_{bg} and T_{bg}) using the 24, 60, 100 and 160 emissivities given in Table 1. For the Local gas component we obtained $P_{vsg} = 1.4^{+0.3}_{-0.7}$, $P_{bg} = 1.4^{+2.0}_{-0.9}$ and $T_{bg} = 16.9^{+2.8}_{-2.0}$ K. For the HVC component we obtained $P_{vsg} = 0.57^{+0.07}_{-0.06}$, $P_{bg} = 13^{+45}_{-9}$ and $T_{bg} = 10.8^{+1.5}_{-1.5}$ K.

In the determination of these parameters we took into account properly the contribution of VSG and BG to all bands. The error given on these parameters are very conservative; they represent the extreme values obtained for these parameters when one considers the errors on the emissivities due to the calibration and correlation uncertainties (taking into account the fluctuation level of the cosmic infrared background). We are confident that our uncertainties on the dust parameters are conservative as the values obtained for the Local component are in complete agreement with the local ISM values ($T_{bg} = 17.6$ K, $P_{bg} = 1$ and $P_{vsg} = 1$).

In the case of a low extinction medium, the BG temperature is related to the strength of the radiation field, the FIR emissivity Q_{FIR} and the UV cross-section Q_{UV} . This relation has been calibrated in the Solar Neighborhood (where $T_{bg} = 17.6$ K and $\chi = 1$) and therefore we can write:

$$T_{bg} = 17.6 \left(\chi \frac{q_{UV}}{q_{FIR}} \right)^{1/(4+\beta)} \quad (4)$$

where $q_{UV} = Q_{UV}^{HVC} / Q_{UV}^{ISM}$. The dust in the HVC is found to be colder ($T_{bg} = 10.8 \pm 1.5$ K) than in the local ISM. The difference in temperature

can be accounted for by a lower radiation field in the HVC than in the Solar Neighborhood due to its distance to the Galaxy and local extinction if the dust emission is arising from high column density clumps. Considering that Complex C is at a distance > 5 kpc, the strength of the radiation field is $\chi < 0.5$ (see ref. [11]). Considering the T_{bg} found, we obtain $q_{FIR}/q_{UV} < 5$ from Eq. 4.

Taking into account the temperature difference, the Big Grain scaling factor P_{bg} is found to be 13_{-9}^{+45} times the local ISM value. There are two possible explanations for such a high value of P_{bg} : 1) unusual dust properties or 2) large amount of gas that would not be traced by the HI. Let's consider the first hypothesis. According to Eq. 3 and considering that the dust-to-gas ratio scales with the gas metallicity (i.e. $Z_d^{HVC}/Z_d^{ISM} = Z_{gas}^{HVC}/Z_{gas}^{ISM}$) which is 0.2 ± 0.1 in Complex C[3, 16, 7], we obtain $q_{FIR} = 65_{-52}^{+398}$. In addition, considering that $q_{FIR}/q_{UV} < 5$, we obtain: $q_{UV} > 13_{-10}^{+103}$. Therefore, to explain the HVC dust parameters one solution would be to have very unusual dust with UV absorption and Far-infrared emission cross-sections much larger than what is observed in the ISM (values of $q_{FIR} \sim 3$ are measured in dense molecular clouds[17]). In this context we favor the second hypothesis which implies that the HVC hydrogen column density would be more than one order of magnitude larger than what is inferred from the HI emission. If we consider ISM type dust ($q_{FIR} = 1$ and $q_{UV} = 1$) the amount of gas increase in hydrogen column density would be 65_{-52}^{+398} times the HI column density.

H α and other ionised atomic lines have been detected in several HVCs. but the ratio HII/HI has been measured[3] to be ~ 0.2 , a fairly typical value for HVCs, too small to explain the dust-to-gas ratio deduced here. In addition H α and HI emission are generally well correlated in velocity but not spatially[8] leading to the current idea that the ionise emission comes from the interaction of the HVC with the Galactic corona. We thus converge towards the conclusion that the dust emission is tracing molecular matter. Molecular gas in HVCs have been unsuccessfully searched in emission[18] and absorption[19]. Two detections of H $_2$ in absorption with FUSE have been reported but the column density are much lower than those of HI[20]. If molecular gas is present in large amount in HVCs it must thus be hidden in a fractal structure with a low surface filling factor. It has been proposed[22] that interstellar matter in regions of low UV radiation field could have a fractal distribution where most of the mass would be hidden in dense gravitationally bound molecular clumps.

The possible existence of large amounts of hidden molecular gas in galaxies would help to solve several problems. Studies of the H I gas dynamics in galaxies point out that the surface density of matter needed to explain the flat rotation curves outside the optical disk is found to be roughly proportional to the surface density of atomic gas[21]. The scaling factors are found to cluster in a range around 10-20 times the HI column density. Similarly, the mass of infalling gas on Milky Way type spirals like the Andromeda galaxy[23] deduced from HI observations is only 10% of what is needed to maintain the observed star formation rate. If our results and interpretation are generalized, cold molecular clumps could make up for the missing baryonic mass. Obviously, the proposed

interpretation of cold dust emission detected in Complex C is far-reaching and open numerous new perspectives on galaxy formation and evolution.

References

- [1] Muller, C. A., Oort, J. H. & Raimond, E. Hydrogène neutre dans la couronne galactique ? 1963, Comptes rendus de l'Académie des Sciences de Paris, 257, 1661.
- [2] van Woerden, H., Wakker, B. P., Schwarz, U. J. & De Boer, K. S. 2004, *High Velocity Clouds*. Kluwer Academic Publishers, Dordrecht.
- [3] Wakker, B. P. et al. Accretion of low-metallicity gas by the milky way. 1999, Nature, 402, 388.
- [4] Sembach, K. R. et al. The deuterium-to-hydrogen ratio in a low-metallicity cloud falling onto the milky way. 2004, ApJS, 150, 387.
- [5] Bournaud, F. & Combes, F. Gas accretion on spiral galaxies: Bar formation and renewal. 2002, A&A, 392, 83.
- [6] Fang, F. et al. The first measurements of galaxy clustering from infrared array camera (IRAC) data of the SPITZER first look survey. 2004, ApJS, 154, 35.
- [7] Tripp, T. M. et al. Complex C: A Low-Metallicity, High-Velocity Cloud Plunging into the Milky Way 2003, AJ, 125, 3122
- [8] Tufte, S. L., Reynolds, R. J. & Haffner, L. M. Wham observations of h alpha emission from high-velocity clouds in the m, a, and c complexes. 1998, ApJ, 504, 773.
- [9] Sembach, K. R. et al. Highly ionized high-velocity gas in the vicinity of the galaxy. 2003, ApJS, 146, 165.
- [10] Wakker, B. P. Distances and metallicities of high- and intermediate-velocity clouds. 2001, ApJS, 136, 463.
- [11] Wakker, B. P. & Boulanger, F. A search for dust in high-velocity clouds. 1986, A&A, 170, 84.
- [12] Bates, B., Catney, M. G. & Keenan, F. P. IRAS maps for a region of sky containing nearby high-velocity gas, identified from IUE spectra. 1988, ApSS, 146, 195.
- [13] Lockman, F. J. & Condon, J. J. The SPITZER space telescope first-look survey: Neutral hydrogen emission. 2005, AJ, 129, 1968
- [14] Miville-Deschenes, M.-A. & Lagache, G. IRIS: A new generation of IRAS maps. 2005, ApJS, 157, 302

- [15] Desert, F. X., Boulanger, F. & Puget, J. L. Interstellar dust models for extinction and emission. 1990, *A&A*, 237, 215.
- [16] Richter, P. et al. The diversity of high- and intermediate-velocity clouds: Complex c versus iv arch. 2001b, *ApJ*, 559, 318.
- [17] Stepnik, B. et al. Evolution of dust properties in an interstellar filament. 2003, *A&A*, 398, 551.
- [18] Wakker, B. P., Murphy, E. M., van Woerden, H. & Dame, T. M. A sensitive search for molecular gas in high-velocity clouds. 1997, *ApJ*, 488, 216.
- [19] Combes, F. & Charmandaris, V. Search for molecular gas in HVCs by HCO⁺ absorption. 2000, *A&A*, 357, 75.
- [20] Richter, P., Sembach, K. R., Wakker, B. P. & Savage, B. D. Molecular hydrogen in high-velocity clouds. 2001a, *ApJ*, 562, L181.
- [21] Hoekstra, H, van Albada, T. S. & Sancisi, R. On the apparent coupling of neutral hydrogen and dark matter in spiral galaxies 2001, *MNRAS*, 323, 453.
- [22] Pfenniger, D. & Combes, F. Is dark matter in spiral galaxies cold gas? ii. fractal models and star non-formation. 1994, *A&A*, 285, 94.
- [23] Thilker, D. A. et al. On the Continuing Formation of the Andromeda Galaxy: Detection of H I Clouds in the M31 Halo 2004, *ApJ*, 601, L39.
- [24] Miville-Deschênes, M. A., Lagache, G., & Puget, J.-L.. Power spectrum of the cosmic infrared background at 60 and 100 μm with IRAS 2002, *A&A*, 393, 749.
- [25] Lagache, G., Dole, H. & Puget, J. L. Modelling infrared galaxy evolution using a phenomenological approach. 2003, *MNRAS*, 338, 555.

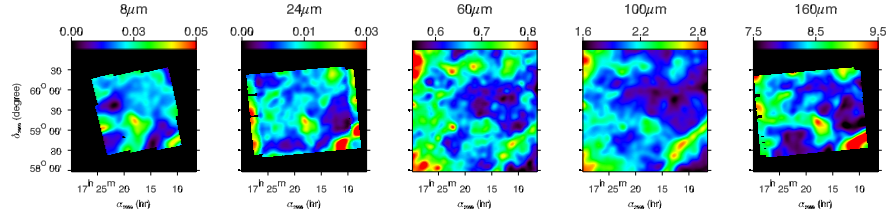


Figure 1: Infrared maps of the XFLS field at 8, 24 and 160 micron from Spitzer and 60 and 100 micron from IRIS. Bright point sources were removed from all maps before convolution by a Gaussian beam to bring them to the GBT 9' FWHM resolution.

Table 1: Infrared-HI correlation

λ	e_{λ}^{Local}	e_{λ}^{HVC}	Calib. uncert.	Noise level	CIB
8 μm	0.018 ± 0.002	0.004 ± 0.001	10%	$0.007 \text{ MJy sr}^{-1}$	$0.006 \text{ MJy sr}^{-1}$
24 μm	0.019 ± 0.002	0.007 ± 0.001	10%	$0.007 \text{ MJy sr}^{-1}$	$0.004 \text{ MJy sr}^{-1}$
60 μm	0.17 ± 0.02	0.059 ± 0.006	10%	0.03 MJy sr^{-1}	$0.048 \text{ MJy sr}^{-1}$
100 μm	0.8 ± 0.1	0.11 ± 0.02	13%	0.06 MJy sr^{-1}	0.09 MJy sr^{-1}
160 μm	1.7 ± 0.3	0.7 ± 0.1	20%	0.07 MJy sr^{-1}	0.12 MJy sr^{-1}

Infrared to HI column density ratio given in $\text{MJy sr}^{-1} (10^{20} \text{ H atoms})^{-1} \text{ cm}^2$ for the Local gas and the HVC, at each wavelength (column 2 and 3). The errors given include the statistical errors on the fit and the uncertainty on the calibration (column 4). To estimate the statistical uncertainty on the parameters e_{λ}^i one needs to estimate the noise level of the $I_{\lambda}(x, y)$. In our case the noise level of the infrared maps is a quadratic combination of the instrumental noise and of the CIB fluctuations. We measured the noise level of the IRIS data as the small-scale fluctuations (smaller than 10 arcminutes) on a $12.5 \times 12.5^{\circ}$ map that include the XFLS field. These values are compatible with the average noise level of the IRIS data product [14]. The noise level of the Spitzer maps has also been estimated by measuring the standard deviation of the small scale fluctuations (scales smaller than 1 arcmin) which we assume to be dominated by noise at all wavelength. Regarding the CIB, at 60 and 100 μm we used the estimate of Miville-Deschênes et al. [24] and at 8, 24 and 160 μm we used estimates given by the model of Lagache et al. [25].

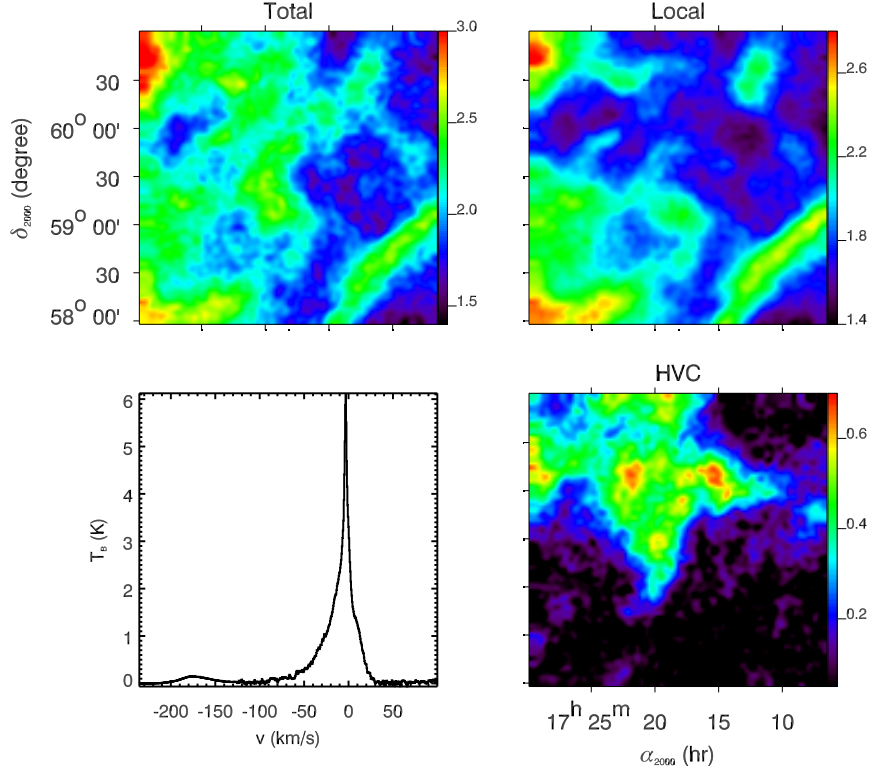


Figure 2: GBT observations at 21 cm of the XFLS field. The bottom-left panel shows the average 21 cm spectrum in the field with one broad local component and one high-velocity component. The top-left panel shows the 21 cm integrated emission in column density using the optically thin approximation. The unit of each maps is 10^{20} cm^{-2} . The top-right and top-bottom panel show the Local and HVC components in the same units. The integrated emission of these two components has been computed by adding all the channels with significant emission (from -60 to 6.6 km s^{-1} for the Local gas and from -210 to -132 km s^{-1} for the HVC).

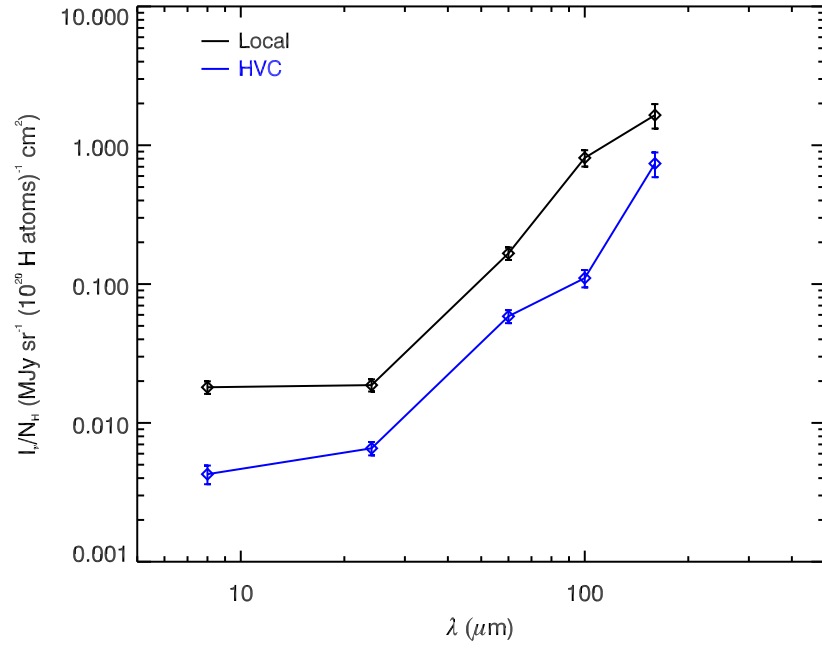


Figure 3: Infrared emissivities for the Local and HVC components shown in Fig. 2. See Table 1 for details.